frontiers | Frontiers in Chemistry

TYPE Original Research
PUBLISHED 17 January 2023
DOI 10.3389/fchem.2022.1089080

OPEN ACCESS

EDITED BY
Feng Gu,
Jiangxi University of Science and Technology, China

REVIEWED BY
Shiyong Zhao,
University of Adelaide, Australia
Dongliang Yan,
Guangxi University for Nationalities, China

*CORRESPONDENCE
Kamel Guedri,
kmguedri@uqu.edu.sa

SPECIALTY SECTION
This article was submitted to Physical Chemistry and Chemical Physics, a section of the journal Frontiers in Chemistry

RECEIVED 03 November 2022
ACCEPTED 30 December 2022
PUBLISHED 17 January 2023

CITATION
Fahim T, Laouedj S, Abderrahmane A, Driss Z, Tag-ElDin ESM, Guedri K and Younis O (2023), Numerical study of perforated obstacles effects on the performance of solar parabolic trough collector.
Front. Chem. 10:1089080.
doi: 10.3389/fchem.2022.1089080

Numerical study of perforated obstacles effects on the performance of solar parabolic trough collector

Tayeb Fahim[1], Samir Laouedj[1], Aissa Abderrahmane[2], Zied Driss[3], El Sayed Mohamed Tag-ElDin[4], Kamel Guedri[5]* and Obai Younis[6]

[1]Materials and Reactive Systems Laboratory (LMSR), Djillali Liabes University, Sidi Bel Abbes, Algeria, [2]Laboratoire de Physique Quantique de la Matière et Modélisation Mathématique (LPQ3M), Université Mustapha Stambouli de Mascara, Mascara, Algeria, [3]Laboratory of Electromechanical Systems (LASEM), National School of Engineers of Sfax, University of Sfax, Sfax, Tunisia, [4]Center of Research, Faculty of Engineering, Future University in Egypt, New Cairo, Egypt, [5]Mechanical Engineering Department, College of Engineering and Islamic Architecture, Umm Al-Qura University, Makkah, Saudi Arabia, [6]Department of Mechanical Engineering, College of Engineering in Wadi Addwasir, Prince Sattam Bin Abdulaziz University, Al-kharj, Saudi Arabia

The current work presents and discusses a numerical analysis of improving heat transmission in the receiver of a parabolic trough solar collector by introducing perforated barriers. While the proposed approach to enhance the collector's performance is promising, the use of obstacles results in increased pressure loss. The Computational Fluid Dynamics (CFD) model analysis is conducted based on the renormalization-group (RNG) k-ε turbulent model associated with standard wall function using thermal oil D12 as working fluid The thermo-hydraulic analysis of the receiver tube with perforated obstacles is taken for various configurations and Reynolds number ranging from 18,860 to 81,728. The results are compared with that of the receiver without perforated obstacles. The receiver tube with three holes (PO3) showed better heat transfer characteristics. In addition, the Nusselt number (Nu) increases about 115% with the increase of friction factor 5–6.5 times and the performance evaluation criteria (PEC) changes from 1.22 to 1.24. The temperature of thermal oil fluid attains its maximum value at the exit, and higher temperatures (462.1 K) are found in the absorber tube with perforated obstacles with three holes (PO3). Accordingly, using perforated obstacles receiver for parabolic trough concentrator is highly recommended where significant enhancement of system's performance is achieved.

KEYWORDS

nanofluid, parabolic trough solar collector, Nusselt number, perforated obstacles, numerical investigation

Highlights

- The flow and thermal characteristics of through solar collector was examined.
- The benefits effects of using perforated baffles to enhance heat transfer was analyzed.
- The position and number of perforations was optimized to obtain the best heat transfer.

Introduction

Growth in global energy demand and the overuse of non-renewable energy sources such as petrol and natural gas have reduced these resources' availability and resulted in harmful severe environmental consequences such as air pollution and global warming (Jamshed et al., 2021; Wu et al., 2021; Zandalinas et al., 2021). Researchers focused on improving technologies involved in renewable energy sources such as solar to address these issues. Solar collectorsuse a heat-exchanging fluid to convert solar power to thermal power. In fact, using the absorber tube absorbs solar light and transfers heat to the absorber fluid. Therefore, the solar collector increases its internal energy, which may be utilized for other purposes (Sayed et al., 2020; Pandey et al., 2021; Shahzad et al., 2021).

Changing traditional working fluids in solar collectors to nanofluids is one of the activities that has gotten a lot of attention in recent years to improve their thermal performance (Aman et al., 2015; Fares et al., 2020; Mourad et al., 2021; Hassan et al., 2022; Khalid et al., 2022). Dehaj et al. (2021) designed and developed an experimental test bench to examine the parabolic trough solar collector (PTSC) efficiency using $NiFe_2O_4$/Water nanofluid as a working fluid. They used a U-shaped absorber tube. Their results show that the PTSC was more effective when the Nickel Ferrite nanofiuid was introduced. In fact, for a volumetric fraction of .05% and a fiow rate of 3 L/min, an efficiency of 51% can be achieved. Farhana et al. (Farhana et al., 2021)investigated the flat plate solar collector efficiency with crystal nano-cellulose (CNC) nanofluid through an experiment. They revealed that the efficiency of the FPSC was enhanced by 2.48% and 8.46% when .5% Al_2O_3 and .5% CNC nanofluids were used, respectively.

Hosseini et al. (Hosseini Seyed and Shafiey Dehaj, 2021) calculated the energetic performance of a PTSC working with Al_2O_3 and GO nanofiuid with a .2% volume fraction. They found that the thermal efficiency of the PTSC was improved by 63.2% and 32.1% when the GO nanofiuid and the Al_2O_3 nanofiuid were used, respectively. Vahidinia et al. (Vahidinia et al., 2021) valued the thermal performance of the PTSC using three types of Syltherm 800 based nanofluids. The first two are Al_2O_3 and SiO_2, and the third is a hybrid nanofluid merging the above two. They illustrated that the exergy and energy performance of the hybrid nanofluid is always the highest. Vital et al. (Vital Caio. et al., 2021) evaluated the thermo-optical properties of TMN nanofluids such as TiN, ZrN, and HfN in an aqueous medium where the nanofluids were used as working fluids for a direct absorption solar collector (DASC). According to their results, the efficiencies of DASC employing TiN, ZrN, and HfN NF are 6.3%, 5.2%, and 5.6%, respectively. They also stated that these enhancements could be achieved without increasing the demands of pumping power by using a low-concentration regime. Ould-Lahoucine et al. (Ould-Lahoucine et al., 2021) proposed a novel technique to identify the ideal height of the rectangular cooling channel for photovoltaic/thermal (PV/T) collector system employing TiO_2-water nanofluid. Before that, they discussed this nanofluid's energy and exergy performances inside the PV/T.

Some researchers focused on nanofluid flow through the absorber tube, which is essentially a channel. Esmaeili et al. (Esmaeili et al., 2019) applied a two-phase model to inspect turbulent flow with both forced and free convection of nanofluid within a 3D rectangular channel (Ajeel Raheem et al, 2022). numerically analyzedthe flow pattern and heat transfer properties of ZnO-water nanofluid within a new channel, where both curved and corrugated profiles for the walls and E-shaped baffles. Berrehal et al. (Berrehal and Sowmya, 2021) analyzed nanofluid flow between two inclined walls using the optimal homotopy asymptotic technique. Ajeel et al. (Ajeel Raheem. et al., 2021) utilized the multi-phase mixture model to evaluate the thermal-hydraulic performance of binary hybrid nanofiuid flowing within a curved-corrugated channel. The results show that using the binary hybrid nanoparticles enhanced the thermal characteristics of the base fluid, thus improving the heat transfer rate in the system. This effect can be furthered by raising the volume fraction or the blockage ratio and reducing the pitch angle.

Recently, a new technique has been employed to enhance nanofluid's heat transport and flow inside channels. It consists of inserting a vortex generator of various shapes and sizes. Their primary purpose is to increase the flow turbulence intensity and eliminate the laminar boundary layer near the walls of the channels. Maadi et al. (Seyed Reza et al., 2021) attempted to enhance the performance of a photovoltaic-thermal system (PV/T) by employing nanofiuid and a wavy-strip insert. The outcomes show that using Al_2O_3water-based nanofiuid and wavy-strip inserts improved the PVT system's thermal efficiency by 12.06% compared to typical PVT. Mashayekhi et al. (Ramin et al., 2020) analyzed the impact of two rows of twisted conical strip inserts on the flow of a water-Al_2O_3 nanofluid in an oval tube. Their study illustrated that inward Co-Conical inserts provide the highest value of heat transport rate, as it can reach 17% higher than tube without inserts. Hamid et al. (Hamid et al., 2019) performed experiments to study the combined impacts of using TiO_2–SiO_2 nanofluids and wire coil inserts on a tube's flow and heat transfer. Chadi et al. (Kamel et al., 2021) studied a diamond-water nanofluid's heat transfer and flow through micro-channels fitted with parallelogram ribs and pie-shaped ribs. The outcomes show that the heat transfer rate was highest when the parallelogram ribs were used. Jing et al. (Jing et al., 2020) underlined the significance of the magnetic field and the shape of heating fins on the flow and heat transport in a rectangular enclosure loaded with nanofluid. Azmi et al. (Azmi et al., 2021) scrutinized the performance of TiO_2–SiO_2/water hybrid nanofluid with various composition ratios flowing inside a tube equipped with wire coil inserts. The outcomes showed that the highest thermal performance factor reached (1.72) with a composition ratio R = .2. In addition, the wire coils can enhance the heat transfer of TiO_2–SiO_2nanofluids by up to 211.75%. Rathnakumar et al. (Rathnakumar et al., 2014) considered improving heat transport turbulent fiow in a tube by equipping it with helical screw louvered rod inserts and employing (CNT)/water nanofiuids at various volume concentrations. The calculations indicated that the helical louvered rod inserts cause augmentation in heat transfer for a certain Reynolds number compared to a plain tube, whereas the friction factor also increased. Kumar et al. (Kumar et al., 2018) and Sundar et al. (Syam et al., 2020) explored the effect of twisted tape and wire coil with core-rod inserts on the heat transport, the friction factor of Fe_3O_4/water nanofiuid fiow inside a double pipe U-bend heat exchanger. Sundar et al. (Syam, Said, Saleh, Singh, Antonio Sousa) calculated the thermal-hydraulic performance of rGO/Co_3O_4 hybrid nanofluid in a plain horizontal tube and another one fitted with longitudinal strip inserts. Their findings indicate that the Nusselt number is boosted by 25.65% when the concentration of hybrid nanoparticles in water is .2%. It is further improved by 110.56% when a straight strip is inserted. However, employing linear strip inserts and hybrid nanofluids results in aninsignificantdrawback in fluid friction. Alnaqi et al.

(Abdulwahab et al., 2021)examined the performance of a solar collector fitted with two twisted tape inserts and loaded with MgO-MWCNT thermal oil-based hybrid nanofluid. Mohammed et al. (Hussein et al., 2019) studied numerically the overall thermo-hydraulic performance of nanofiuids in forced convection fiow inside circular tubes fitted with divergent and convergent conical rings inserts. According to their results, the divergent ring inserts produced a 365% enhancement in the performance criteria, making them the best option. Sheikhzadeh et al. (Ghanbar et al., 2019) examined an ethylene-glycol-based hybrid nanofluid's thermodynamic and flow properties in a rectangular channel with turbulators with various wing forms. The result shows that the trapezoidal wings with a volume fraction of .6% provide the best heat transfer performance considering fluid flow.

In recent years, various combinations of nanofluids as well as affecting parameters on the different structures are taken for analysis-oriented with the thermal application such as solar collectors. They have been considered and developed, as a result, effective enhancement of heat transfer achieved by many research works (Rathnakumar et al., 2014; Kumar et al., 2018; Ghanbar et al., 2019; Hamid et al., 2019; Hussein et al., 2019; Jing et al., 2020; Ramin et al., 2020; Syam et al., 2020; Syam, Said, Saleh, Singh, Antonio Sousa; Abdulwahab et al., 2021; Azmi et al., 2021; Kamel et al., 2021; Seyed Reza et al., 2021). To the authors' knowledge, no research has been done on the examination of the position and number of perforations to optimize and to enhance the performance of a photovoltaic-thermal system (PV/T) by employing nanofiuid and a wavy-strip insert. Accordingly, the aim of this study is to improve heat transfer inside parabolic through solar receiver using two different passive methods, perforated obstacles and nanoparticles. This work also investigates the effects of perforated obstacles inserted centrally inside the absorber of a PTC for various cases. Inserts are placed centrally, the diameters of the perforations are large, they are fixed to the top surface of the receiver tube, and their dimensions are much smaller than those found in the literature. In reality, inserting holes in obstacles aids fluid mixing by breaking the thermal boundary layer and aids fluid mixing due to the non-uniform circumferential heat flow profile on the receiver; hence the thermal performance is remarkably improved. The motivated work aims to answer to the following research questions.

- What is the effect of the perforated obstacles on heat transfer in a solar parabolic trough collector using nanofluids?
- What is the impact of the position and number of these perforations on the temperature of thermal oil fluid used?
- What are the benefits effects of using perforated baffles to enhance heat the performance evaluation criteria.
- How friction factor values decrease with the increase in the number of these holes?

Model description

Physical model

Figure 1 depicts the solar parabolic system's schematic and the collector's receiver. The parabolic trough collector (PTC) concentrates the direct sunlight on the bottom perimeter of the parabolic trough receiver (PTR). In contrast, the top perimeter of the PTR is exposed to non-concentrated solar irradiation (Figure 1A). Figure 1 shows a cross-section drawing of the PTR (b). A glass cover protects the stainless-steel absorber tube. The space between the metal tube and the glass cover is constantly vacuumed to reduce heat loss. The focused solar energy travels through the glass cover and lands on the metal tube's outer surface. The concentrated solar energy is absorbed and transformed into heat by the metal tube. The heat is conveyed to the heat transfer fluid by conduction and convection modes. The receiver model employed in this study intends to improve the heat transmission performance of PTR by introducing absorber tubes with perforated barriers (Figures 2, 3). Table 1 shows the geometrical characteristics of PTR and perforated barriers. Table 2 also depicts the thermophysical parameters of the working fluid (Thermal oil D12), perforated barriers, and absorber tube.

Boundary conditions

The boundary conditions are as follows.

- Fluid inlet:

$$V_{x=}V_{in}, \quad V_{y=}V_z = 0 m/s, \tag{1}$$

$$T_f = T_{in} = 400\,K\ (L = 0,\ 00^0 \le \varphi \le 360^\circ \tag{2}$$

- At the walls

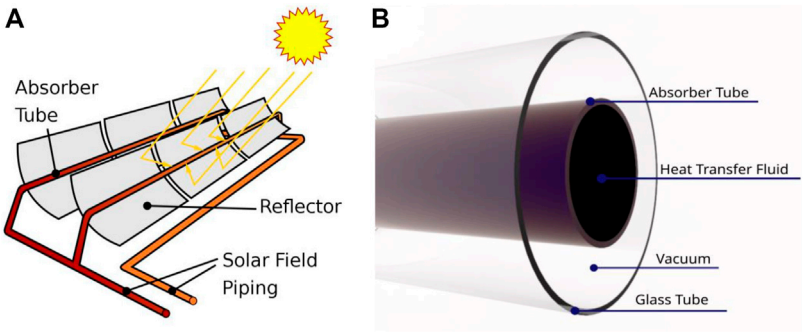

FIGURE 1
(A) Parabolic trough collector (PTC). **(B)** Cross-sectional diagram of the parabolic trough receiver (PTR) (Wang et al., 2015).

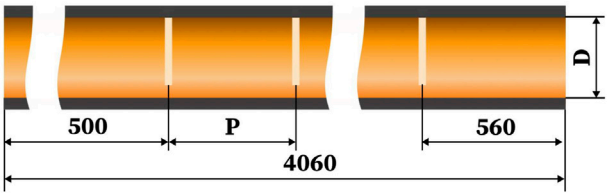

FIGURE 2
The receiver's longitudinal segment with perforated obstruction inserts.

The upper half perimeter of the metal tube is exposed to the uniform heat flux qt, which is calculated as:

$$q_t = DNI \times TGE \times AMT = 1000 \times 0.95 \times 0.96$$
$$= 912 W/m^2 \left(0 \le L \le 4.06 m, 0^o \le \varphi \le 180^o\right) \quad (3)$$

Where DNI, TGE, and AMT are the solar irradiation, the glass envelope transmissivity, and the metal tube absorptivity, respectively. The concentrated solar irradiation qcal was computed by. (Kamel et al., 2021) (Figure 4). The lower half perimeter of the metal tube is subjected to the heat flux qb, which is calculated as:

$$q_b = q_{cal}\ ;\ \left(0 \le L \le 4.06\ m,\ 180^\circ \le \varphi \le 360^\circ\right) \quad (4)$$

- Fully formed conditions are enforced at the fluid outflow.
- In this study, the outer absorber wall is subjected to a non-uniform heat flux estimated using the Monte Carlo Ray Tracing (MCR) method and a DNI of 1000 W/m2. Figure 4 depicts the variation of the heat flux distribution along the bottom-half perimeter of the absorber tube for present and Hachicha et al. (Hachicha et al., 2013) models. Using the current calculation, the heat flux distribution pattern of the absorber tube is plotted in Figure 5.

Numerical model

Numerical method

The computational fluid dynamics (CFD) modeling technique was used in this work. The finite volume technique (FVM) is used to discretize the equations. The resulted equations system is solved numerically by employing the commercial package software ANSYS-FLUENT (Release 17.1). The RNG k-ε turbulence model is employed to simulate the turbulent flow of Thermal oil D12 in the solar collector's absorber tube. Second-order UPWIND and QUICK methods are used for discretizing the convective components in momentum and energy equations. For dealing with pressure-velocity coupling, the SIMPLEC method is

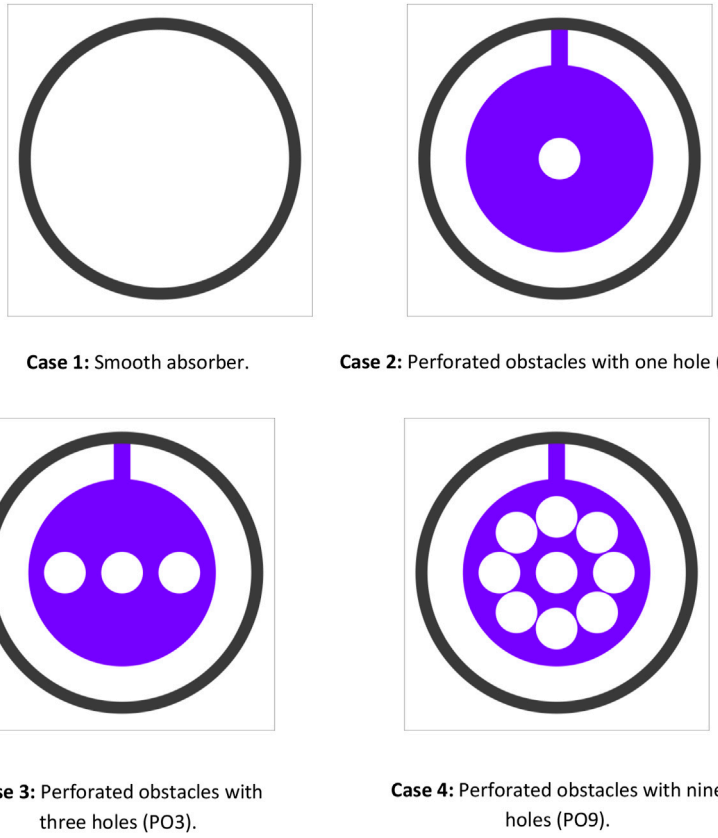

FIGURE 3
Cross-section of the receiver tube with perforated obstacles and smooth absorber.

TABLE 1 The PTR model parameters and perforated obstacles.

Parameter	Values	Reference
Length of the absorber (m)	4.06	Wu et al., 2014a, Wu et al., 2014b
Internal diameter of the metal tube (m)	.064	
External diameter of the metal tube (m)	.07	
Internal diameter of the Glass cover (m)	.117	
External diameter of the Glass cover (m)	.12	
Glass envelope transmissivity	.95	
Metal tube absorptivity	.96	
Obstacle diameter (mm)	46	
Perforated obstaclesthickness (mm)	2	
Diameter of the perforation (mm)	10	
Distance between two consecutive perforated obstacles (mm)	128	
Number of perforated obstacles in the absorber tube	25	

utilized. For all equations, the convergence threshold is 10–6. GAMBIT version 2.2 is used to generate and the mesh of the physical model (Figure 6).

Governing equations

The instantaneous Navier Stokes equation is used to generate the RNG k-turbulent model by using a mathematical approach known as "renormalization group" (RNG) methods (Gnielinski, 1976; Yakhot et al., 1992). The values of k (turbulent kinetic energy) and ε (turbulent dissipation rate) are determined by equations:

$$\rho\left(\frac{\partial k}{\partial t}+\overline{u_j}\frac{\partial k}{\partial x_j}\right)=\frac{\partial}{\partial x_j}\left[\left(\mu+\frac{\mu_t}{\sigma_{k\,(RNG)}}\right)\frac{\partial k}{\partial x_j}\right]+P_k-\rho\varepsilon \tag{5}$$

$$\rho\left(\frac{\partial \varepsilon}{\partial t}+\overline{u_i}\frac{\partial \varepsilon}{\partial x_i}\right)=\frac{\partial}{\partial x_j}\left[\left(\mu+\frac{\mu_t}{\sigma_{\varepsilon\,(RNG)}}\right)\frac{\partial \varepsilon}{\partial x_j}\right]+\frac{\varepsilon}{k}\left(C_{1\varepsilon(RNG)}P_k-C_{2\varepsilon(RNG)}\rho\frac{\varepsilon}{k}\right) \tag{6}$$

Where

$$P_k=-\rho\overline{u_i'u_j'}\frac{\partial \overline{u_i}}{\partial x_j} \tag{7}$$

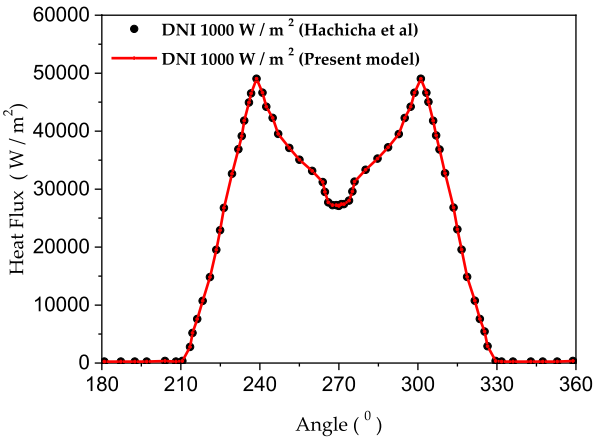

FIGURE 4
Heat flux distribution variation along the bottom half perimeter of the absorber tube.

$$C_{2\varepsilon(RNG)}=\frac{C_{2\varepsilon}+C_\mu\eta^3\left(1-\frac{\eta}{\eta_0}\right)}{1+\beta\eta^3} \tag{8}$$

$$\eta=\frac{k}{\varepsilon}\left(2S_{ij}S_{ij}\right)^{1/2} \tag{9}$$

The turbulent viscosity μ_t is calcluated as:

$$\mu_t=\rho C_\mu\frac{k^2}{\varepsilon} \tag{10}$$

Where the parameter ρ represents the fluid's density.

S_{ij} denotes the strain tensor rate and is defined as:

$$S_{ij}=\frac{1}{2}\left(\frac{\partial \overline{u_i}}{\partial x_j}+\frac{\partial \overline{u_j}}{\partial x_i}\right) \tag{11}$$

Table 3 summarizes the model constants used.

Results and discussion

Grid independency

Numerous calculations were undertaken to determine the total number of grid points required to create an array adequate for measuring flux and thermal field in order to justify the simulation solution's accuracy and consistency. Table 4 illustrates the evolution of the average Nusselt number as a cell number function for Reynolds numbers ranging from 10^4 to 10^6.

TABLE 2 Thermophysical properties of the working fluid, perforated obstacles, and absorber tube.

	Working fluid (thermal oil D12)	Perforated obstacles and absorber tube (stainless steel)	Reference
Density (Kg/m3)	679	8,027	Solutia, (1998)
Specific heat (J/Kg.K)	2,571	500	
Thermal conductivity (W/m.K)	.091	20	
Viscosity (N.s/m2)	.000346	—	

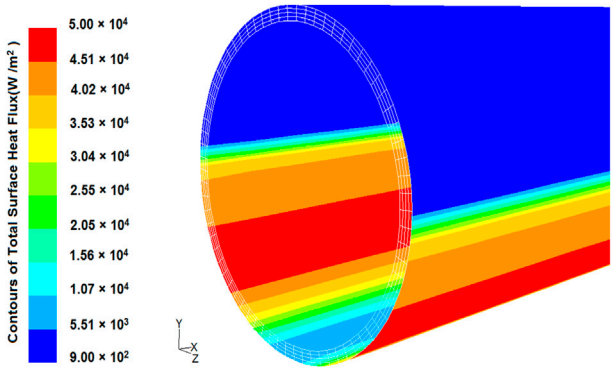

FIGURE 5
Heat flux distribution on the absorber tube surface (current study).

Code validation

To determine the validity and correctness of the model and numerical solution used in this inquiry, the Nusselt number generated in this study is compared to the Nusselt number computed using the Gnielinski correlation (Petukhov et al., 1970). Gnielinski devised the following equation to get the Nusselt number of a smooth tube:

$$Nu_D = \frac{(f/8)(R_{eD} - 1000)Pr}{1 + 12.7(f/8)^{1/2}(Pr^{2/3} - 1)}; For 3000 \le Re \le 5 \times 10^6 and 0.5 \le Pr \le 2000 \quad (12)$$

Where the Petukhov friction correlation is as used in (Gee and Webb, 1980):

$$f = (0.790 \ln Re_D - 1.64)^{-2}; \ For\ 3000 \le Re \le 5 \times 10^6 \quad (13)$$

By flowing the PTR heat transfer fluid through a metal tube, the heat transfer properties of the fluid are studied. The Nu_{avg}, Re, and heat transfer coefficient (h) read are as follows:

$$Nu_{avg} = \frac{h.D}{\lambda} \quad (14)$$

$$Re = \frac{D.v}{\nu} \quad (15)$$

$$h = \frac{q''}{T_{t,a} - T_{f,a}} \quad (16)$$

The Darcy friction factor in turbulent flow regime is as defined in (Amina et al., 2017):

$$f = \frac{2.\Delta P.D}{L.\rho.v^2} \quad (17)$$

Using the relation between the pressure and shear forces, the above expression can be written as:

$$f = \frac{8.\tau_w}{\rho.v^2} \quad (18)$$

To verify the quality of the computational model employed in this study, the Gnielinski and Petukhov correlations for the Nusselt number and friction factor are utilized to evaluate the simulation of heat transfer and flow properties of the thermal oil D12 in the absorber tube. Figure 7 and Figure 8 show the friction factor and Nusselt number comparisons between the numerical results and the correlations for smooth absorber, respectively. The maximum deviation value of the numerical results was found to be around 7.8% and 15%, and the minimum deviation equals 18% and 11% for the Nusselt number and friction factor, respectively. The heat transfer and flow properties are clearly in agreement with the correlations.

Effect of perforated obstacles on heat transfer

As seen in Figure 9, changes in Reynolds number (Re) generate fluctuations in Nusselt number, which has values of 18860 (v = 15 m/s), 44007 (v = 35 m/s), and 81728 (v = 65 m/s) when using thermal oil D12 as working fluid. The Nusselt number approximately linearly rises in proportion to the Reynolds number; this enhancement is caused by introducing perforated barriers, which improve the heat transfer area. The vortex flow was caused by fluid mixing given by the perforated barriers, and enhanced turbulent intensity at high values of Re leads the thermal boundary layer to be destroyed. The highest gain is seen in absorber tubes with three holes and perforated barriers (PO3). The average Nusselt number improves by 115 percent compared to the standard case with the smooth absorber. Perforated barriers with one hole (PO1) are the second most successful example, with an average Nusselt number enhancement of 108 percent.

In contrast, perforated barriers with nine holes (PO9) have the smallest Nusselt number enhancement, which equals 54 percent. From Figure 10, it can be observed that the smooth case has the

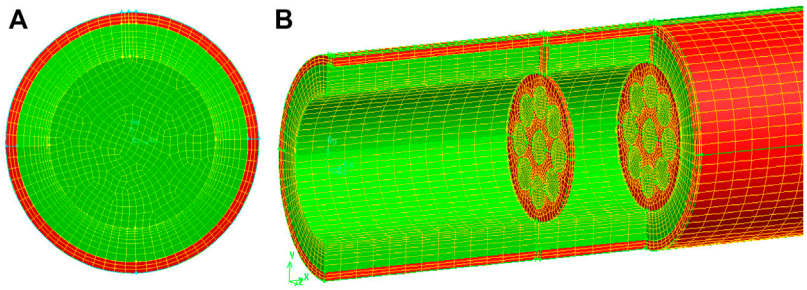

FIGURE 6
3D mesh of the computational domain.

TABLE 3 Model constants.

C_{μ}	$C_{1\varepsilon(RNG)}$	$C_{2\varepsilon(RNG)}$	$\sigma_{k\,(RNG)}$	$\sigma_{\varepsilon\,(RNG)}$	η_0	β
.0845	1.42	1.68	.7194	.7194	4.38	.012

TABLE 4 Mesh effect on the average Nusselt number.

N_{cells}					
	294600	307200	330400	354400	
Re	Nu				|δmax|
10^4	148.123	150.021	149.613	150.461	1.57%
10^5	222.104	226.371	226.719	229.004	3.10%
10^6	259.121	258.223	259.942	260.781	.64%

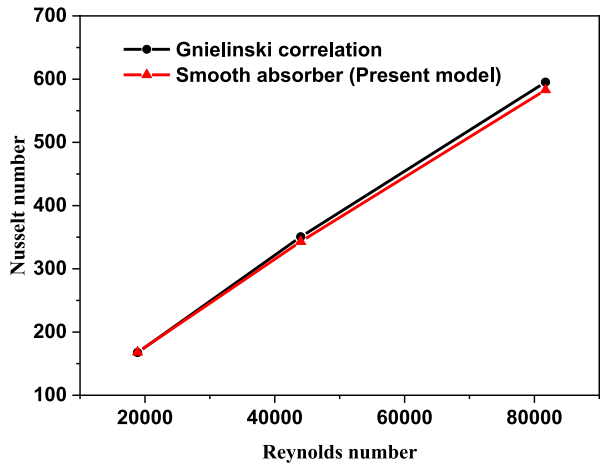

FIGURE 7
Nussle number with Gnielinski correlation.

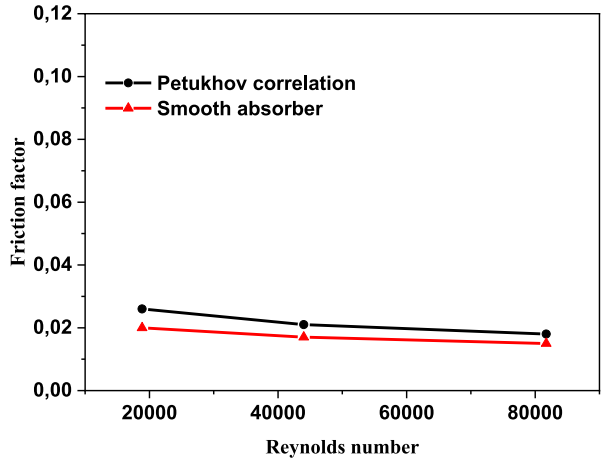

FIGURE 8
Friction factor with Petukhov correlation.

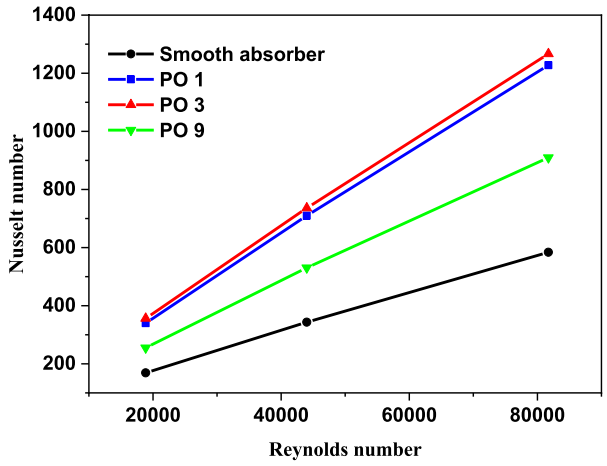

FIGURE 9
Nu variation in the absorber vs. Reynolds number (P/D = 2).

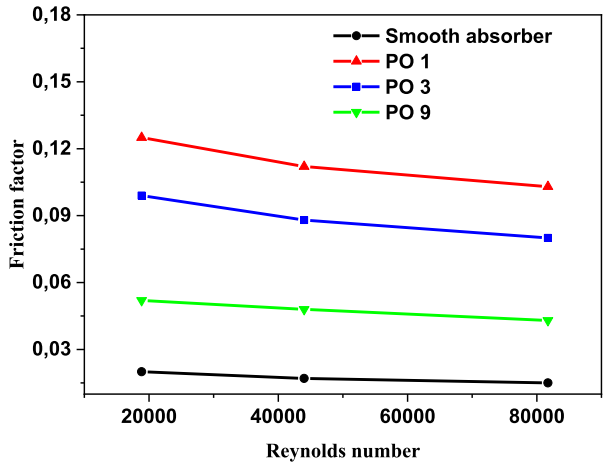

FIGURE 10
Variation in absorber tube's friction factor vs. Reynolds number (P/D = 2).

smallest friction factor of all the cases investigated in this study. The largest friction factor is obtained when perforated barriers with one hole (PO1) are used, followed by perforated barriers with three holes (PO3) and perforated barriers with nine holes (PO9) in the second and third cases, respectively. These higher values are caused by the whirling flow generated by the inserts that function as an obstruction. Figure 11 displays the heat transfer fluid average temperature distribution on sectional planes (y-axis and z-axis) along the entire length of the absorber tube with and without impediments. At the exit, the temperature reaches its peak. Higher temperatures (462.1 K) are achieved in the absorber tube with perforated barriers with three holes (PO3), followed by (461.56 K) for perforated barriers with one hole (PO1), and 454.92 K for perforated barriers with nine holes (PO9). Figure 12 shows the temperature distributions of the PTR absorber tube on two distinct cross-sections with Re = 81728 for various scenarios.

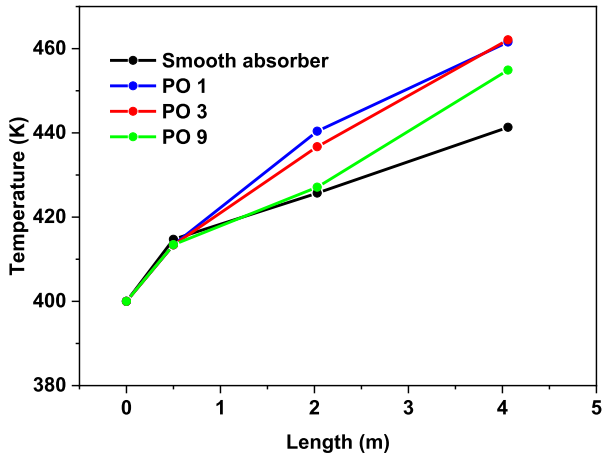

FIGURE 11
Variation in absorber tube's average temperature and without perforated obstacles (Re = 81728, v = .65 m/s).

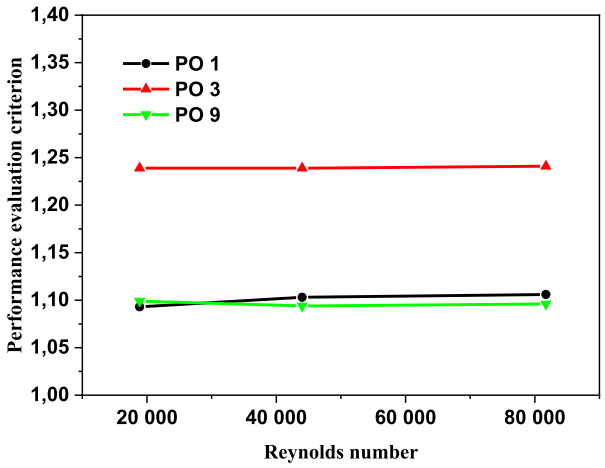

FIGURE 13
Performance evaluation criteria variation vs. Re number.

Thermal performance analysis

To enhance heat transfer efficiency, it is required to assess both heat transfer and flow resistance concurrently. As a result, as stated below (Xiangtao et al., 2017), the performance evaluation criteria (PEC) are universal assessment tools that reflect a heat transfer unit's overall performance. The thermal performance criterion was calculated as the ratio of the

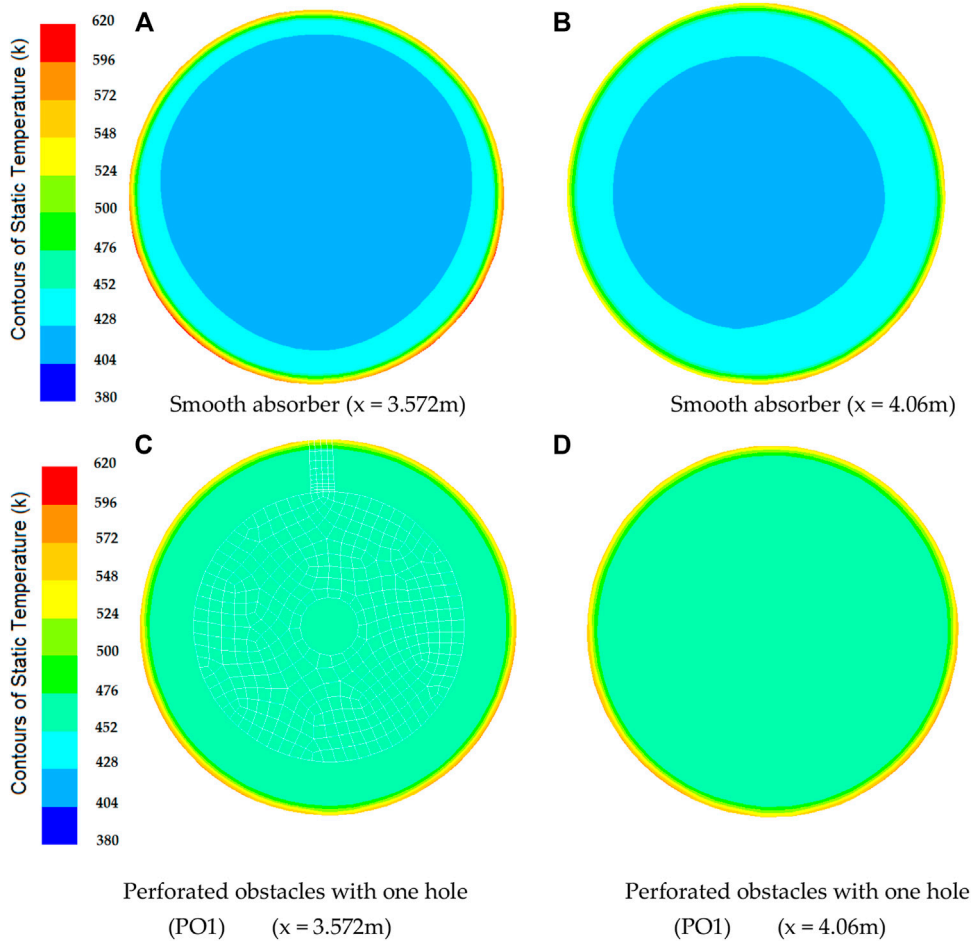

FIGURE 12
Temperature distribution of absorber tube of PTR at cross-sections with Re = 81728.

TABLE 5 Comparison with literature studies with inserts in the receiver of a parabolic trough solar collector and the present study.

Cas	Insert type	Increase (%) Nu	PEC	Method	Reference
Present study	Perforated obstacles	115	1,24	CFD	
Gong Xiangtao	Pin fin arrays	9	1.12	CFD	Mwesigye et al. (2016)
Aggrey Mwesigye	Twisted tape	58.8	1.02	CFD	Mwesigye et al. (2014)
Aggrey Mwesigye	Perforated plate	8–133.5	.44–1.05	CFD	

dimensionless Nusselt number to the dimensionless friction factor.

$$PEC = \frac{Nu/Nu_0}{(f/f_0)^{1/3}} \quad (19)$$

where (Nu0) and (Nu1) represent the smooth absorber case (f0).

Figure 13 illustrates the fluctuation of performance evaluation criteria (PEC); when the PEC values exceed one, it indicates that the inserts have a favorable influence on heat transfer. It is notable that the perforated barriers give a heat transfer boost over the smooth tube. The perforated barriers with three holes had the greatest PEC value (PO3).

Table 5 includes the obtained increase in the Nusselt number (Nu) and in the performance evaluation criteria (PEC). Data has been estimated according to the results of these papers. Moreover, this table shows the method of every study. These studies more specifically, present lower performance evaluation criteria (PEC) compared to the present study. According to the final results, the use of perforated obstacles leads to 1.24% performance evaluation criteria (PEC) enhancement.

Conclusion

The effect of utilizing varied perforated barriers on the thermal performance of parabolic through the solar receiver is computationally investigated in this work. The following observations could be drawn from this work.

- In comparison to the reference case (smooth absorber), the greatest increase in Nusselt number was 115%, and it was attained by the perforated obstacles with three holes (PO3), followed by 108% for the perforated obstacles with one hole (PO1), while the perforated obstacles with nine holes (PO9) achieved the minimum enhancement of 54%.
- Friction factor values decrease with the increase in the number of holes on obstacles. In the case of the tube without perforated obstacles, friction factor values are less than all the friction factor values with perforated obstacles inserts.
- The perforated barriers in the absorber tube increase the Nusselt number while decreasing the friction factor.
- The highest PEC value was obtained for the perforated obstacles with three holes (PO3).
- The temperature of the heat transfer fluid reaches its maximum value near the exit, while temperatures as high as 462.1 K are obtained in the absorber tube with perforated barriers with three holes (PO3).

Data availability statement

The original contributions presented in the study are included in the article/Supplementary Material, further inquiries can be directed to the corresponding author.

Author contributions

All authors listed have made a substantial, direct, and intellectual contribution to the work and approved it for publication. KG, TF, SL, AA: Formal analysis, investigation and writing-original draft. ZD, ET-E, OY: Formal analysis and supervision. MZB-F: Funding acquisition, software and revision. KG, ET-E: Funding acquisition, validation and revision. KG, ET-E: Funding acquisition, resources and revision. TF, SL, AA: Funding acquisition, validation and revision. ZD, ET-E, OY: Conceptualization, editing and revision.

Acknowledgments

The authors extend their appreciation to the Deanship for Research and Innovation, Ministry of Education in Saudi Arabia for funding this research work through the project number: IFP22UQU4331317DSR151.

Conflict of interest

The authors declare that the research was conducted in the absence of any commercial or financial relationships that could be construed as a potential conflict of interest.

Publisher's note

References

Abdulwahab, A., Alsarraf, J., and Al-Rashed, A. (2021). Hydrothermal effects of using two twisted tape inserts in a parabolic trough solar collector filled with MgO-MWCNT/thermal oil hybrid nanofluid. *Sustain. Energy Technol. Assessments Volume* 47, 101331. doi:10.1016/j.seta.2021.101331

Ajeel Raheem, K., Sopian, K., and Zulkifli, R. (2022). A novel curved-corrugated channel model: Thermal-hydraulic performance and design parameters with nanofluid. *Int. Commun. Heat Mass Transf.*

Ajeel Raheem., K., Zulkifli, R., Sopian, K., Fayyadh, S., Ahmad, F., and Ibrahim, A. (2021). Numerical investigation of binary hybrid nanofluid in new configurations for curved-corrugated channel by thermal-hydraulic performance method. *Powder Technol.* 385, 144–159. doi:10.1016/j.powtec.2021.02.055

Aman, M., Solangi, K., Hossain, M., Badarudin, A., Jasmon, G., Mokhlis, H., et al. (2015). A review of Safety, Health and Environmental (SHE) issues of solar energy system. *Renew. Sustain. Energy Rev.* 41, 1190–1204. doi:10.1016/j.rser.2014.08.086

Amina, B., Abdelylah, B., Samir, L., and Solano, J. P. (2017). Numerical analysis of compound heat transfer enhancement by single and two-phase models in parabolic through the solar receiver. *J. Mech.* 23 (1), 55–61.

Azmi, W. H., Abdul Hamid, K., Ramadhan, A. I., and Shaiful, A. I. M. (2021). Thermal hydraulic performance for hybrid composition ratio of TiO2–SiO2 nanofluids in a tube with wire coil inserts. *Case Stud. Therm. Eng.* 25, 100899. doi:10.1016/j.csite.2021.100899

Berrehal, H., and Sowmya, G. (2021). Heat transfer analysis of nanofluid flow in a channel with non-parallel walls. *J. Mech. Sci. Technol.* 35, 171–177. doi:10.1007/s12206-020-1216-y

Dehaj, M. S., Rezaeian, M., Davoud Mousavi, B., Shamsi, S., and Salarmofrad, M. (2021). Efficiency of the parabolic through solar collector using NiFe2O4/Water nanofluid and U-tube. *J. Taiwan Inst. Chem. Eng.* 120, 136–149. doi:10.1016/j.jtice.2021.02.029

Esmaeili, H., Armaghani, T., Abediniand, A., and Pop, I. (2019). Turbulent combined forced and natural convection of nanofluid in a 3D rectangular channel using two-phase model approach. *J. Therm. analysis Calorim.* 135, 3247–3257. doi:10.1007/s10973-018-7471-9

Fares, R., Abderrahmane, A., Mebarek-Oudina, F., Ahmed, W., Rashad, A. M., Sahnoun, M., et al. (2020). Magneto-free convectiveof hybrid nanofluid inside a non-Darcy porous enclosure containing an adiabatic rotating cylinder. E. *nergy Sources Part A Recovery Util. Environ. Eff.* 136 (4), 1–16.

Farhana, K., Kadirgama, K., Hussein Mohammed, A., Ramasamy, D., Samykano, M., and Saidur, R. (2021). Analysis of efficiency enhancement of flat plate solar collector using crystal nano-cellulose (CNC) nanofluids. *Sustain. Energy Technol. Assessments* 45, 101049. doi:10.1016/j.seta.2021.101049

Gee, D. L., and Webb, R. L. (1980). Forced convection heat transfer in helically rib-roughened tubes. *Int. Heat. Mass Transf.* 23, 1127–1136. doi:10.1016/0017-9310(80)90177-5

Ghanbar, S. A., Faezeh, N. B., Ali Akbar, A. A., and Pourfattah, F. (2019). Wings shape effect on behavior of hybrid nanofluid inside a channel having vortex generator. *Heat Mass Transf.* 55, 1969–1983. doi:10.1007/s00231-018-2489-x

Gnielinski, V. (1976). New equations for heat and masstransfer in turbulent pipe and channel flow. *Int. J. Chem. Eng.* 16, 359–e68.

Hachicha, A. A., Rodriguez, I., Capdevila, R., and Oliva, A. (2013). Heat transfer analysis and numerical simulation of a parabolic trough solar collector. *Appl. Energy* 111, 581–592. doi:10.1016/j.apenergy.2013.04.067

Hamid, A., Azmi, W. H., Mamat, R., and Sharma, K. V. (2019). Heat transfer performance of TiO2–SiO2 nanofluids in a tube with wire coil inserts. *Appl. Therm. Eng.* 152 (4), 275–286. doi:10.1016/j.applthermaleng.2019.02.083

Hassan, M. K., Alqurashi, I. M., Salama, A. E., and Mohamed, A. F. (2022). Correction to: Investigation the performance of PV solar cells in extremely hot environments. *J. Umm Al-Qura Univ. Eng. Archit.* 13, 86. doi:10.1007/s43995-022-00007-9

Hosseini Seyed, M. S., and Shafiey Dehaj, M. (2021). An experimental study on energetic performance evaluation of a parabolic trough solar collector operating with Al2 O3/water and GO/water nanofluids. *nergy* 234, 121317. doi:10.1016/j.energy.2021.121317

Hussein, M., Abuobeida, I. A., Vuthaluru, H., and Liu, S. (2019). Two-phase forced convection of nanofluids flow in circular tubes using convergent and divergent conical rings insertsInternational Communications in Heat and Mass Transfer 101, 10–20.

Jamshed, W., Eid, M. R., Aissa, A., Mourad, A., Nisar, K. S., Shahzad, F., et al. (2021). Partial velocity slip effect on working magneto non-Newtonian nanofluids flow in solar collectors subject to change viscosity and thermal conductivity with temperature. *PLoS ONE* 16, e0259881. doi:10.1371/journal.pone.0259881

Jing, D., Hu, S., Hatami, M., Xiao, Y., and Jia., J. (2020). Thermal analysis on a nanofluid-filled rectangular cavity with heated fins of different geometries under magnetic field effects. *J. Therm. Analysis Calorim.* 139, 3577–3588. doi:10.1007/s10973-019-08758-9

Kamel, C., Belghar, N., Guerira, B., Lachi, M., and Chikhi, M. (2021). Effect of the addition of pie-shaped ribs and parallelogram ribs in micro-channels on thermal performance using diamond-water nanofluid. *SN Appl. Sci.* 3, 316. doi:10.1007/s42452-021-04292-2

Khalid, A. M. A., Obaid, A., Nima, S., Hikmet, Ş. A., Shi, F., Samah, E. A., et al. (2022). Installation of rectangular enclosures filled with phase change nanomaterials on the thrombus walls of a residential building to manage solar radiation in different seasons of the year. *J. Build. Eng.* 57, 104732. doi:10.1016/j.jobe.2022.104732

Kumar, B., Gaurav, P. S., Kumar, M., and Patil, A. K. (2018). A review of heat transfer and fluid flow mechanism in heat exchanger tube with inserts. *Chem. Eng. Process. - Process Intensif.* 123 (1), 126–137. doi:10.1016/j.cep.2017.11.007

Mourad, A., Aissa, A., Mebarek-Oudina, F., Al-Kouz, W., and Sahnoun, M. (2021). Natural convection of nanoliquid from elliptic cylinder in wavy enclosure under the effect of uniform magnetic field: Numerical investigation. *Eur. Phys. J. Plus* 136, 429. doi:10.1140/epjp/s13360-021-01432-w

Mwesigye, A., Bello-Ochende, T., and Meyer, J. P. (2016). Heat transfer and entropy generation in a parabolic trough receiver with wall-detached twisted tape inserts. *Int. J. Therm. Sci.* 99, 238–257. doi:10.1016/j.ijthermalsci.2015.08.015

Mwesigye, A., Bello-Ochende, T., and Meyer, J. P. (2014). Heat transfer and thermodynamic performance of a parabolic trough receiver with centrally placed perforated plate inserts. *Appl. Energy* 136, 989–1003. doi:10.1016/j.apenergy.2014.03.037

Ould-Lahoucine, C., Ramdani, H., and Driss, Z. (2021). Energy and exergy performances of a TiO2-water nanofluid-based hybrid photovoltaic/thermal collector and a proposed new method to determine the optimal height of the rectangular cooling channel. *Sol. Energy* 221, 292–306.

Pandey, A., Kumar, R. R., Kalidasan, B., Laghari, I. A., Samykano, M., Kothari, R., et al. (2021). Utilization of solar energy for wastewater treatment: Challenges and progressive research trends. *J. Environ. Manag.* 297, 113300. doi:10.1016/j.jenvman.2021.113300

Petukhov, B. S., Irvine, T. F., and Hartnett, J. P. (1970). Heat transfer and friction in turbulent pipe flow with variable physical properties. *Adv. Heat. Transf.* 6, 503–564.

Ramin, M., Arasteh, H., Toghraie, D., Motaharpour, H., Keshmiri, A., and Afrand, M. (2020). Heat transfer enhancement of water-Al2O3 nanofluid in an oval channel equipped with two rows of twisted conical strip inserts in various directions: A two-phase approach. *Comput. Math. Appl.* 79 (8), 2203–2215. doi:10.1016/j.camwa.2019.10.024

Rathnakumar, P., Mayilsamy, K., Suresh, S., and Murugesan, P. (2014). Laminar heat transfer and pressure drop in tube fitted with helical louvered rod inserts using CNT/water nanofluids. *J. Bionanoscience* 8 (11), 160–170. Number 3. doi:10.1166/jbns.2014.1225

Sayed, E. T., Wilberforce, T., Elsaid, K., Rabaia, M. K. H., Abdelkareem, M. A., Chae, K.-J., et al. (2020). A critical review on environmental impacts of renewable energy systems and mitigationstrategies: Wind, hydro, biomass and geothermal. *Sci. Total Environ. Sci. Total Environ.* 766, 144505. doi:10.1016/j.scitotenv.2020.144505

Seyed Reza, M., Ali, N., Solomin, E., Hoahn, S., Wongwises, S., and Mahian, O. (2021). Performance improvement of a photovoltaic-thermal system using a wavy-strip insert with and without nanofluid. *Energy Vol.* 234 (1), 121190. doi:10.1016/j.energy.2021.121190

Shahzad, F., Jamshed, W., Sathyanarayanan, S. U. D., Aissa, A., Madheshwaran, P., and Mourad, A. (2021). Thermal analysis on Darcy-Forchheimer swirling Casson hybrid nanofluid flow inside parallel plates in parabolic trough solar collector: An application to solar aircraft. *Int. J. Energy Res.* 45, 20812–20834. doi:10.1002/er.7140

Solutia. Combined heating & cooling highly stable heat transfer fluid. Heat transfer fluids by SOLUTIA. Applied Chemistry, Creative Solution. GROUP PROVOC T.B.S 10-19 (12/98) E. 1998, Available online: http://twt.mpei.ac.ru/TTHB/HEDH/HTF-D12.PDF (12/98.1998).

Syam Sundar, L., Said, Z., Saleh, B., Singh Manoj, K., and Antonio Sousa, C. M. (2020). Combination of Co3O4 deposited rGO hybrid nanofluids and longitudinal strip inserts: Thermal properties, heat transfer, friction factor, and thermal performance evaluations. *Sci. Eng. Prog.* 100695.

Syam, S., Yihun, T. S., Said, Z., Singh, M., and Punnaiah, V. (2020). Energy, efficiency, economic impact, and heat transfer aspects of solar flat plate collector with Al2O3 nanofluids and wire coil with core rod insertsSustainable. *Energy Technol. Assessments* 40, 100772.

Vahidinia, F., Khorasanizadeh, H., and Aghaei, A. (2021). Comparative energy, exergy and CO2 emission evaluations of a LS-2 parabolic trough solar collector using Al2O3/SiO2-Syltherm 800 hybrid nanofluid. *energy Convers. Manag.* 245, 114596. doi:10.1016/j.enconman.2021.114596

Vital Caio ., V. P., Farooq, S., Renato Araujo, E., Rativa, D., and LuisGomez-Malagon, A. (2021). Numerical assessment of transition metal nitrides nanofluids for improved performance of direct absorption solar collectors. *Appl. Therm. Eng.* 190, 116799. doi:10.1016/j.applthermaleng.2021.116799

Wang, F. Q., Tan, J. Y., Ma, L. X., and Wang, C. C. (2015). Effects of glass cover on heat flux distribution for tube receiver with parabolic trough collector system. *Energy Convers. Manag.* 90, 47–52. doi:10.1016/j.enconman.2014.11.004

Wu, X., Deng, H., Li, H., and Guo, Y. (2021). Impact of energy structure adjustment and environmental regulation on air pollution in China: Simulation and measurement research by the dynamic general equilibrium model. *Technol. Forecast. Soc. Change* 172, 121010. doi:10.1016/j.techfore.2021.121010

Wu, Z. Y., Lei, D. Q., Yuan, G. F., Shao, J. J., Zhang, Y. T., and Wang, Z. F. (2014). Structural reliability analysis of parabolic trough receivers. *Appl. Energy**2014*** 123, 232–241. doi:10.1016/j.apenergy.2014.02.068

Wu, Z. Y., Li, S. D., Yuan, G. F., Lei, D. Q., and Wang, Z. F. (2014). Three-dimensional numerical study of heat transfer characteristics of parabolic trough receiver. *Appl. Energy**2014*** 113, 902–911. doi:10.1016/j.apenergy.2013.07.050

Xiangtao, G., Fuqiang, W., Haiyan, W., Tan, J., Lai, Q., and Han, H. (2017). Heat transfer enhancement analysis of tube receiver for parabolic trough solar collector with pin fin arrays inserting. *Sol. Energy* 144, 185–202.

Yakhot, V., Orszag, S. A., Thangam, S., Gatski, T. B., and Speziale, C. G. (1992). Development of turbulence models for shear flows by a double expansion technique. *Phys. Fluids A* 4 (7), pp1510–1520. doi:10.1063/1.858424

Zandalinas, S. I., Fritschi, F. B., Mittler, R., and Global, W. (2021). Global warming, climate change, and environmental pollution: Recipe for a multifactorial stress combination disaster. *Trends Plant Sci.* 26, 588–599. doi:10.1016/j.tplants.2021.02.011